Journal of Materials Chemistry C

Facile synthesis and magnetic phase transformation of Nd–Fe–B nanoclusters by oxygen bridging†

Chang Woo Kim,[a] Young Hwan Kim,[b] Umapada Pal[c] and Young Soo Kang*[a]

We demonstrate a facile chemical approach for fabricating Nd–Fe–B nanoclusters through oxygen bridging. The Nd–Fe–B nanoclusters comprised of small aggregated particles (∼2 nm diameter) could be successfully synthesized using sodium borohydride, a conventional reducing agent. The three-step process consists of the formation of Fe–B primary particles through borohydride reduction and the reduction of Nd cations over the Fe–B particles under hydrophilic conditions in coordination with oxygen. Finally, a reductive annealing process in an H_2 atmosphere allowed the oxidized Nd phase in Nd–Fe–B nanoclusters to be reduced and diffuse into the Fe–B primary phase to form ternary $Nd_2Fe_{14}B$ intermetallic nanoparticles. The magnetic behaviors of both the primary Nd–Fe–B nanoclusters and the final intermetallic $Nd_2Fe_{14}B$ phase have been studied. Through reductive annealing, the as-grown amorphous Nd–Fe–B nanoclusters of soft magnetic behaviour could be transformed to a crystalline intermetallic $Nd_2Fe_{14}B$ phase of highly ferromagnetic nature. The mechanism of formation of the lanthanide based intermetallic phase has been discussed. The proposed method of synthesis can lead to a simple route for the otherwise difficult fabrication of lanthanide-based intermetallic ternary nanostructures.

Introduction

Lanthanide (Ln) related materials and their nanostructures are gaining growing importance in the fields of coordination chemistry of lanthanide and Ln-based solid-state chemistry.[1] Lanthanides play critical roles in various realms such as the production of high quality phosphors and up-conversion materials due to their large magnetic anisotropy, fabrication of integrated optical systems, and materials with outstanding electrochemical characteristics arising from their 4f orbital.[2] Among the Ln-related materials, ferromagnetic Nd–Fe–B has attracted much attention as a candidate for high performance permanent magnets with a high saturation magnetization (M_s = 16 kG), a near-ideal maximum energy product value (($BH)_{max}$ = 14.0 MGOe), and a high curie temperature (T_c = 586 K).[3] However, due to their incompatibility with other elements, and chemical instabilities like rapid oxidation,[3] it is extremely difficult to manufacture stable Nd and Sm-related intermetallic magnetic nano-materials. Despite recent advances in synthesizing ternary alloys, there are few reports on the fabrication of lanthanide-based ternary alloy systems, due to highly negative

reduction potentials of the lanthanides; although they offer several advantages over mono- and bi-metallic systems. Until now, large scale physical techniques such as mechanical alloying, sputtering and melt spinning processes have been widely used for synthesizing permanent magnetic materials. However, in most of the cases, the final products obtained from these typical fabrication processes are of little use due to their restricted grain size, uncontrolled morphology, and wide particle size distribution.[3]

Recently, solution-based colloidal synthesis approaches have been reported as superior methods to manipulate the size, shape, and composition of metal, metal oxide, and semiconductor nanostructures of different morphologies.[4] Adopting those approaches, monometallic, bimetallic, even tri-metallic nanoparticles have been fabricated successfully. As an example, Sun and Liu et al.[5] have reported the synthesis of bimetallic nanoparticles of controlled size and shape with enhanced magnetic properties. O'Brien et al.[6] have demonstrated the fabrication of a large variety of composition tunable binary superlattice structures in the solution phase. Several binary and ternary magnetic materials such as SmCo and SmCoFe have also been generated in the last few years due to their strong application potential as high performance permanent magnetic materials. Nevertheless, there exist very few reports on the chemical synthesis and phase transition behaviors of Ln-related magnetic materials due to the difficulty in finding appropriate precursors and chemical instability of Ln.[7] Moreover, there is no decisive outcome on the ferromagnetic behaviors of the

[a] Korea Center for Artificial Photosynthesis, Department of Chemistry, Sogang University, Seoul, 121-742, Republic of Korea. E-mail: yskang@sogang.ac.kr; Fax: +82 2 701 0967; Tel: +82 2 701 6379

[b] Department of Functional Layers, GMBU e.V, D-01317 Dresden, Germany

[c] Instituto de Fisica, Universidad Autonoma de Puebla, Puebla 72570, Mexico

This journal is © The Royal Society of Chemistry 2013

J. Mater. Chem. C, 2013, 1, 275–281 | 275

Ln-based magnetic materials obtained by polyol synthesis or thermal decomposition of Ln precursors.[3]

Here we report on a general approach for the synthesis of Ln–transition metal (TM)–boron intermetallic nanoclusters in aqueous medium along with their formation pathway, and magnetic phase transformation behaviors. This procedure should facilitate the otherwise difficult synthesis of Ln-based nanoclusters and inter-metallic nanostructures in aqueous medium overcoming the main hindrance associated with highly negative reduction potential.

Experimental

Synthesis of Nd–Fe–B nanoclusters

For the synthesis of Fe–B primary particles, we used a 250 mL three-necked round bottom flask as the reactor with two inlets being used for injecting metal ion solution and high-purity Ar gas, and the other as an outlet of exhaust for releasing the generated hydrogen gas. All the precursors used for synthesis were of the reagent grade. About 0.02 mol of $NaBH_4$ was dissolved in 150 mL of nanopure H_2O (18.2 MΩ) under magnetic stirring in an argon atmosphere. A freshly prepared solution of $FeCl_2 \cdot 4H_2O$ (0.014 mol in 50 mL of H_2O) was then added dropwise to the previous solution under stirring. After 30 min, the product was collected by centrifugation, washed several times with distilled water and acetone, and dried under inert atmosphere.

For the synthesis of Nd–Fe–B nanoclusters, the same procedure was followed; however, about 0.002 mol of $NdCl_3 \cdot 6H_2O$ was added into the sodium borohydride solution. The pH of the solution was controlled to 10 by adding an appropriate amount of 1 M NaOH solution.

Reductive annealing of as-synthesized Nd–Fe–B nanoclusters

To achieve crystallinity, the as-synthesized Nd–Fe–B nanoclusters were annealed at 500 or 950 °C for 2 h in a tubular vacuum furnace. Before heating, the sample chamber was evacuated to 2×10^{-5} mbar and an Ar + H_2 (4%) mixture gas was purged. The temperature of the furnace was raised either to 500 °C or to 950 °C at the rate of 7 °C min^{-1}. The mixture gas flow was maintained at 100 cc min^{-1} during the annealing process. After 2 h, the furnace was cooled down to room temperature.

Nd–Fe–B nanocluster characterization

The morphology and elemental composition of the samples were studied using a JSM-6700F field emission scanning electron microscope (FESEM, JEOL) with Oxford JEM-2010 energy dispersive spectroscopy (EDS) facility attached. High resolution transmission electron microscopic (HRTEM) images and selected area electron diffraction (SAED) patterns of the samples were obtained in a JEOL JEM2010 TEM operated at 200 keV accelerating voltage. UV-visible absorption spectra of the Nd precursor solution before and after reduction were recorded using a Varian, Cary UV-visible spectrometer. The nature and surface charge density of the primary (Fe–B) and final (Nd–Fe–B) particles were measured by a Zeta Potential

Analyzer ver. 2.18 (Brookhaven Instruments Corp). The composition and chemical state of the components of the nanoclusters were studied using X-ray photoelectron spectroscopy (XPS, MULTILAB 2000). The crystal structure of the as-synthesized and the H_2-reduced Nd–Fe–B nanoclusters were identified using the Cu-Kα radiation source ($\lambda = 0.154056$ nm) of a Philips X'Pert-MPD X-ray diffractometer. Thermo-magnetic analysis (TMA), *i.e.* recording the magnetic force *versus* temperature for the samples, was performed in a thermogravimeter containing a microbalance with magnetic field gradient positioned below the sample. For TMA, the samples were heated and cooled down at a rate of 7 °C min^{-1}. Magnetization curves of the samples were recorded at room temperature (RT) in a SQUID magnetometer (Quantum Design, MPMS XL 7) after fixing the powder samples on the sample holder with wax to prevent their physical movement.

Results and discussions

Our synthesis procedure is based on the successive reduction of Fe and Nd salts and the coordination between metal and oxygen in their aqueous solutions using sodium borohydride ($NaBH_4$) as the reducing agent. Precipitation of metals from their aqueous solution requires the chemical reduction of their cations. The chemical reduction of metal cations is based on the change in Gibbs free energy of the reaction, $\Delta G^0 = -nFE^0$ (F is the Fermi energy of the metal and E^0 is the standard reduction potential), which must be favorable for electron transfer.[8] The standard reduction potential of $B(OH)_3$ or BH_4^-, which act favorably in several redox systems, $E^0 = -0.481$ eV, and any metal ion with E^0 higher than -0.481 eV can be reduced to neutral atom in aqueous borohydride solution. For example, the reduction of TM cations such as Fe^{2+}/Fe^0 [$E^0 = -0.447$ eV] and Co^{2+}/Co^0 [$E^0 = -0.28$ eV] can be easily performed using borohydride solution. The main problem related to the chemical synthesis of Ln-based nanoclusters is the reduction of trivalent Ln cations. Due to highly negative reduction potential of Ln^{3+} cations, metal ions like Nd^{3+}, Sm^{3+}, and Pr^{3+} are very difficult to be reduced even using very strong reducing agents like borohydride derivatives. In the case of Nd, the reduction potential for Nd^{3+}/Nd^0 is $E^0 = -2.323$ eV, which is much lower than the borohydride system, $B(OH)_3$–BH_4^- [$E^0 = -0.481$ eV]. Finding a new synthesis approach that overcomes this problem is therefore essential.

We have developed a reaction pathway that can overcome the energy requirement problem associated with the conversion of Ln^{3+} ion to Ln^0 *via* co-reduction of TM cations. The approach follows our recently developed technique on the surface chemistry of supported nanoparticles.[9] Under hydrophilic conditions, a surface-mediated reduction can take place in which strong nucleophiles are formed on the surface of primary nanophase. Metal cations could be reduced to metal atoms on the surface of the primary particles causing the deprotonation of hydroxyl ligands (–OH) with the reducing agent in aqueous medium. Influence of the pH value of the reaction solution has been widely studied to manipulate Ln-oxide and Ln-hydroxide nanocrystals obtained using Ln^{3+} cations.[7b,10] During reaction in

276 | *J. Mater. Chem. C*, 2013, **1**, 275–281

This journal is © The Royal Society of Chemistry 2013

|

an aqueous borohydride system, the nucleation of TM particles occurs simultaneously with their aggregation into large nanoparticles, as documented in several review articles.[8a,11] Although it is difficult to observe each of these steps individually, the primary nucleation can be driven by the solution itself, in which the metal ions are reduced.[8a] In the case of TM–Ln bimetallic systems, it is expected that the TM nucleates and grows as primary nanoparticulates at the initial stage of the reaction in an aqueous borohydride system, as the standard reduction potential of TM^{2+}/TM^0 is more positive than that of Ln^{3+}/Ln^0.[8] The Ln^{3+} cations can be bonded to the TM particles and reduced to Ln^0 under hydrophilic conditions; *i.e.* the secondary nucleation of Ln can be catalyzed by the presence of the primary TM nanoparticles with lower activation energy than that initially required for Ln^{3+} reduction. The secondary phase can be formed on the surface of the primary particles and can grow along with during the synthesis process. During the reduction process, the metallic Ln can form a secondary phase, possibly suppressing the growth of primary particles, resulting in discrete structures as can be seen from the HRTEM image of the Nd–Fe–B nanoclusters with the composition Nd (10 at.%), Fe (70 at.%) and B (20 at.%) presented in Fig. 1. The effect of TM on the reduction of Ln cations is very clear from the UV-visible spectra (Fig. 6) of hydrated Nd(III) solution before and after the addition of TM salt, which is discussed later.

The X-ray photoelectron spectra of the as-synthesized nanoclusters with and without Nd are presented in Fig. 2. Considering the Fermi level as reference ($E_f = 0$), emission bands related to Fe $2p_3$ in Fe–B or elemental Fe should be observed at about 706.6 eV.[12] However, the Fe $2p_3$ and O 1s
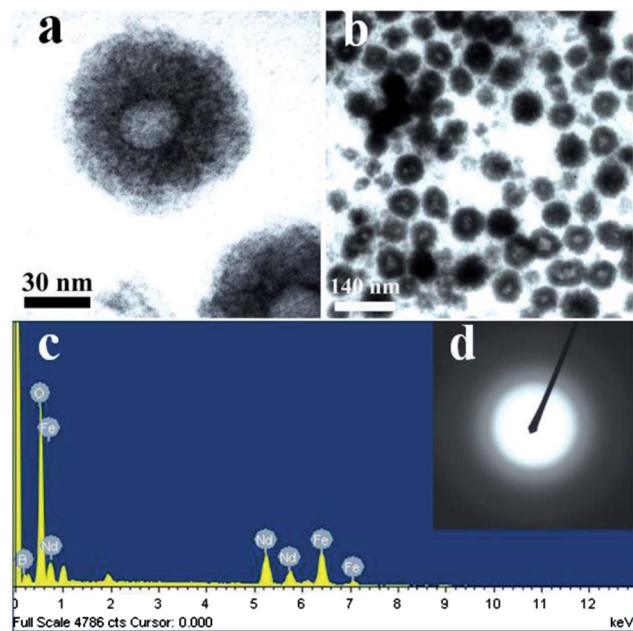

Fig. 1 Typical high (a) and low (b) resolution TEM images of as-synthesized Nd–Fe–B nanoclusters. The high resolution TEM image revealed that each nanocluster consists of several smaller particles. The typical EDS spectrum (c) and SAED pattern (d) of the as-synthesized Nd–Fe–B nanoclusters with the composition Nd (10 at.%), Fe (70 at.%) and B (20 at.%) are presented.
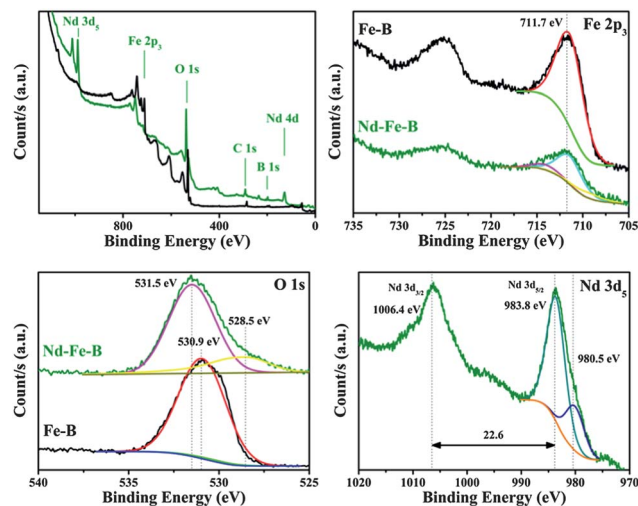

Fig. 2 Survey (top-left), and high resolution XPS spectra of as-synthesized Fe–B (black) and as-synthesized Nd–Fe–B (green) samples showing O 1s, Fe $2p_3$, and Nd $3d_5$ regions with corresponding peak deconvolutions. While the 530.9 eV position of O 1s peak in the Fe–B sample corresponds to the formation of Fe–O, the components at 531.5 eV and 528.5 eV in the as-synthesized Nd–Fe–B sample correspond to the FeB–O and Nd–O states, respectively.

emission bands in our as-synthesized primary (Fe–B) particles are observed at about 711.7 eV and 530.9 eV, respectively. Such high energy shifts of the binding energies of valence electrons of O 1s and Fe $2p_3$ orbitals are due to the formation of Fe–O and Fe–OH chemical bonds. Observed binding energy shifts of Fe $2p_3$ and O 1s orbitals are typical of Fe(II) and Fe(III) in iron oxide and hydroxides.[12,13] Such a high energy shift of the binding energy of Fe $2p_3$ suggests that the surface of the as-synthesized primary Fe–B nanoparticles is nucleophilic due to the existence of oxygen and hydroxyl ions. Under hydrophilic conditions, a surface-mediated reduction process can take place in which strong nucleophiles are formed on the surface of the primary nanoparticle, causing the deprotonation of hydroxyl ligands (–OH). The nucleophilic parts (–O–) can then lower the activation energy and interact with metal cations in the solution.[9] In comparison with the as-synthesized primary particles (Fe–B), the as-synthesized Nd–Fe–B nanoparticles revealed O 1s emission with components at about 531.5 eV and 528.5 eV, which
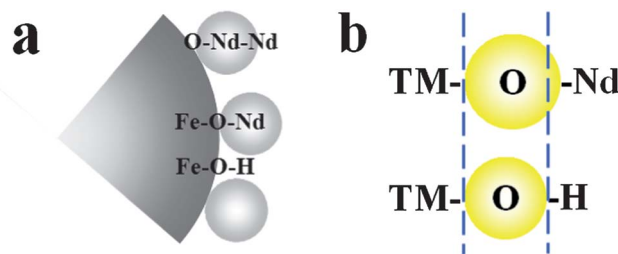

Fig. 3 Schematic presentation of chemical bonding between Ln and TM through oxygen bridging (a), and electron distribution of oxygen in TM–O–Nd and TM–O–H (b). Note that due to the shift of the electron cloud towards Nd, the binding energy of O observed in the XPS spectrum of FeB–O–Nd is lower than the binding energy of O in FeB–O–H.

|

correspond to the typical binding energies of oxygen in FeB–O and Nd–O chemical bonds, respectively.[11] We attribute these observations primarily to the formation of the oxygen bridge between Nd and Fe atoms in the form of Nd–O–Fe (Fig. 3).

The O 1s binding energy in different oxides varies between 528.0 and 533.5 eV depending on the degree of ionicity of the metal-oxygen bonds.[14] Some oxides such as La_2O_3 and Ce_2O_3 exhibit very low O 1s binding energies, which lie in-between 529.5 and 528.0 eV, due to their high ionicity (>90%). Higher ionicity of the counter cation in an oxide decreases the binding energy of the core element.[13] Therefore, valence electrons of oxygen atoms would be shifted more toward H in TM–O–H than towards Nd in TM–O–Nd. As the result, the ejection of core electrons of O from TM–O–H would be more difficult than from TM–O–Nd. Observation of the O 1s emission peak at a lower binding energy in the case of TM–O–Nd than in TM–O–H is the result of the above mentioned phenomenon. A schematic presentation of oxygen bridging between Fe and Nd in our as-synthesized Nd–Fe–B sample and valence electron distribution

Table 1 Core level binding energies of elemental transitions in as-synthesized Fe–B and Nd–Fe–B nanoclusters

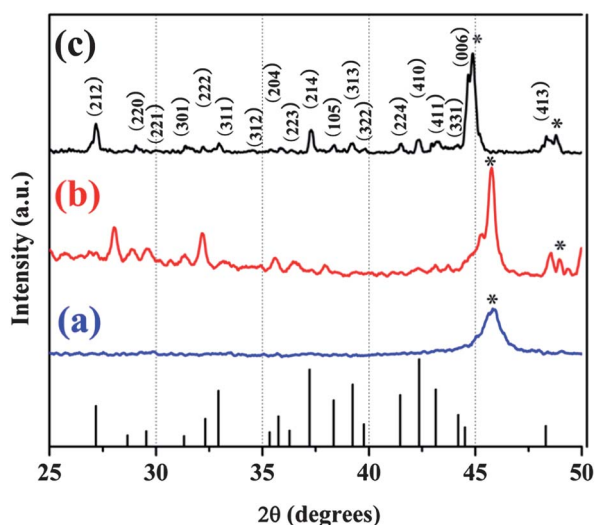|	Binding energy (eV)		
Element	Fe–B phase	Nd–Fe–B nanocluster	Reported binding energy (eV)
Fe 2p$_3$	711.7	711.7	706.6 (metallic Fe–Fe, ref. 12)
O 1s			529.9 (ref. 12)
Fe–O–H	530.9	531.5	530.2 (ref. 12 and 13a)
Fe–O–Nd	—	528.5	529 (Nd$_2$O$_3$, ref. 12)
Nd 3d$_5$			
Nd–Nd	—	980.5	980.9 (metallic Nd–Nd, ref. 12)
Nd–O	—	983.8	984.2 (Nd oxide, ref. 12)

Fig. 4 XRD patterns of Nd–Fe–B nanoclusters: as-synthesized (a), after reductive annealing at 500 °C for 2 h (b), and after reductive annealing at 950 °C for 2 h (c). Standard peak positions for Nd$_2$Fe$_{14}$B (JCPDS 86-0273) are indicated at the bottom. Peaks corresponding to the Fe–B phase are marked by (*, JCPDS 75-1065).
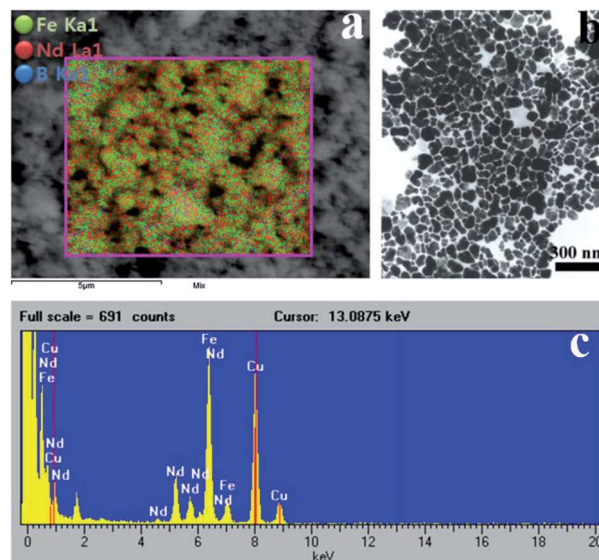

Fig. 5 FESEM micrograph and elemental mapping (a), TEM image (b), and EDS spectrum (c) of the Nd–Fe–B nanoparticles after annealing at 950 °C for 2 h in a reducing atmosphere.

of oxygen in it are shown in Fig. 3. Deconvolution of the Nd 3d$_5$ XPS peak in our as-synthesized Nd–Fe–B sample indicates that it consists of metallic Nd–Nd (at 980.5 eV) and Nd–O (at 983.8 eV) components (Fig. 2).[11–14] Table 1 summarizes the XPS binding energies of all the elemental transitions in as-synthesized primary (Fe–B) and as-synthesized secondary (Nd–Fe–B) nanoclusters.

Our XPS results strongly suggest that Ln^{3+} ions can be catalyzed, bonded and then reduced on the surface of the primary particles. Despite their highly negative reduction potentials, the Ln^{3+} cations could be easily reduced to Ln atoms with the help of borohydride reductor together with the electrostatic interaction of the negatively charged TM–B surface. The electrostatic interaction of the Ln^{3+} ions with the negatively charged surface of Fe–B primary particles has also been confirmed through zeta
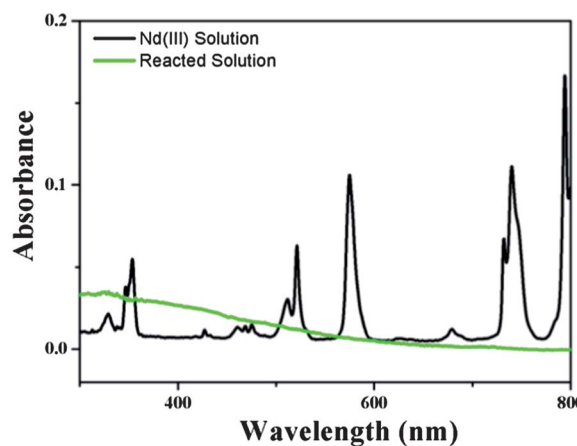

Fig. 6 UV-visible spectra of aqueous Nd precursor solution (black) and the residue collected 30 min after the addition of TM salt (green). The peaks appeared in the Nd precursor sol correspond to the Nd^{3+} ions.
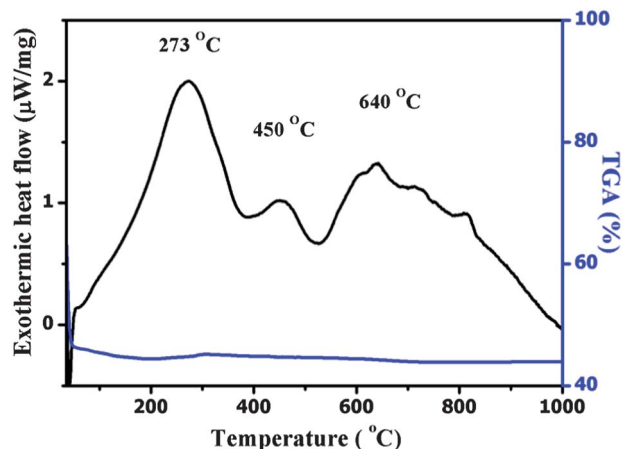
278 | *J. Mater. Chem. C*, 2013, **1**, 275–281

This journal is © The Royal Society of Chemistry 2013

Fig. 7 DSC (black) and TGA (blue) traces of the as-synthesized Nd–Fe–B nano-clusters recorded in an Ar atmosphere with a heating rate of 10 °C min^{-1}.

Fig. 8 The magnetization curves of the as-grown Nd–Fe–B nanoclusters (black), after reductive annealing at 500 °C (blue) and after reductive annealing at 950 °C (green).

potential analysis of the samples (see ESI, Fig. S1†). Based on the results of XRD (Fig. 4) and EDS (Fig. 5) analysis of the samples, it is clear that the synthesized Nd–Fe–B nanoclusters with the composition Nd (10 at.%), Fe (70 at.%) and B (20 at.%) after reductive annealing at 950 °C turns out to be the inter-metallic $Nd_2Fe_{14}B$ compound.

The effect of oxygen bridging on the reduction of Ln cations is very clear from the UV-vis absorption spectra (Fig. 6) of the Nd(III) precursor solution containing borohydride before and after the addition of the TM precursor. Formation of primary particles (Fe–B) and nucleation of the secondary phase over them are very clear from the TEM images (see ESI, Fig. S2 and S3†) and the UV-vis spectrum of the final product. Differential scanning calorimetry (DSC) (Fig. 7) and XRD traces revealed the transformation process of the as-grown nanoclusters to the final inter-metallic compound. The DSC thermogram of the as-synthesized Nd–Fe–B nanoclusters revealed three exothermic peaks at about 273, 450, and 640 °C. While the first exotherm at 273 °C might be attributed to an amorphous to crystalline transition of iron oxide in the sample, the second exotherm (at 450 °C) might be due to subsequent bonding and coarsening of crystalline particles. The last exotherm at 640 °C can be attributed to the formation of neodymium oxide in the sample.[15] The reduction-diffusion process during reductive annealing of as-grown Nd–Fe–B nanoclusters at high temperature (e.g. 950 °C) passes through all these three transitions. From the XRD patterns presented in Fig. 4, we can also see that the as-synthesized Nd–Fe–B clusters are mostly amorphous and they crystallize to the ferromagnetic $Nd_2Fe_{14}B$ tetragonal phase (JCPDS 86-0273) on thermal annealing in a reducing atmosphere. Therefore we believe that under reductive annealing, the as-grown amorphous nanoclusters of the mixed phase pass through several compositional changes at subsequent temperatures, reaching finally to the inter-metallic $Nd_2Fe_{14}B$ composition at a temperature higher than 800 °C.

The magnetic behaviors of the as-synthesized and reductively annealed samples were studied using a Superconducting Quantum Interference Device (SQUID) magnetometer at RT. As
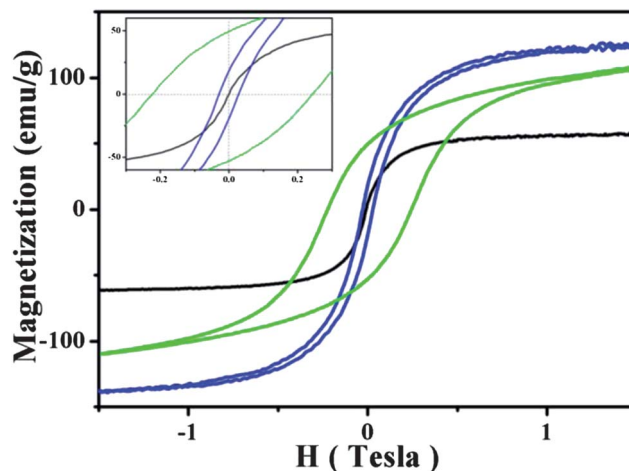
expected, the as-synthesized amorphous Nd–Fe–B clusters revealed their soft-magnetic behavior (Fig. 8). After the reductive annealing treatment at 950 °C, the nanostructures were converted fully to the ferromagnetic phase. The hysteresis loops of the annealed samples revealed drastically higher coercivity in comparison with that of the as-synthesized nanoclusters. The coercivity (H_c) of the sample reductively annealed at 950 °C (and obviously of $Nd_2Fe_{14}B$ phase) was about 2400 Oersted (O_e), with remanance (M_r) of 51 emu g^{-1}, and saturation magnetization (M_s) as high as 110 emu g^{-1}. The results suggest that Nd after reduction diffuses into the primary TM phase, changing it to a ferromagnetic material.

Gong et al.[16] have reported a higher M_s value (153 emu g^{-1}) for their nanostructured $Nd_2Fe_{14}B$ sample of an average grain size of ∼50 nm with coercivity of 7.4 kOe. Hou et al.[3c] have reported the synthesis of $SmCo_5$ nanomagnets of about 32 nm grain size with room temperature M_s on the order of 55 emu g^{-1}, a coercivity of about 8.0 kOe and remanence in between 40 and 50 emu g^{-1}. It must be noted that though the TEM estimated average (ca.) particle size (p) of our reductively annealed Nd–Fe–B nanostructures (i.e. $Nd_2Fe_{14}B$ phase) was about 90 nm, their XRD estimated (using Scherrer formula

$$p = \frac{0.9\lambda}{\beta \cos \theta},$$

where λ is the X-ray wavelength and β is the full width at half maximum of the diffraction peak) average grain size was about 35.0 nm only. Though the M_s and coercivity of our $Nd_2Fe_{14}B$ nanostructures are lower than the values of the $Nd_2Fe_{14}B$ phase reported by Gong et al.[16] due to smaller grain size and higher magnetocrystalline anisotropy, the values are much higher than the corresponding values of nanocrystalline $SmCo_5$ reported by Hou et al.,[3c] which is believed to be a better candidate for the fabrication of permanent magnets. The results presented in this article demonstrate how the Ln–transition metal (TM)–boron inter-metallic compound exhibiting near-ideal magnetic behaviour can be synthesized through a chemical reduction
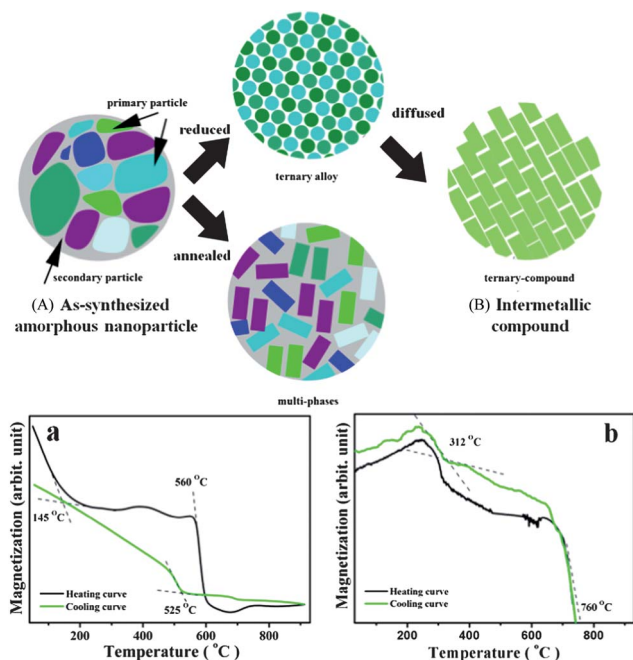
Fig. 9 Schematic representation of the formation process of an intermetallic ternary alloy from amorphous nanoclusters (A and B). TMA curves of the as-synthesized and reductively annealed Nd–Fe–B alloy are presented in (a) and (b), respectively.

process despite the otherwise difficult synthesis of Ln based inter-metallic nanostructures.

The magnetic moment and its temperature dependence are the most significant characteristics of magnetic materials. The formation process of binary and ternary magnetic alloys can be confirmed through their ferromagnetic–paramagnetic transition temperature, known as the Curie temperature, T_c, estimated from their thermo-magnetic analysis (TMA). TMA results presented in Fig. 9 reveal the formation of the final product through the formation of binary and ternary alloys, and the temperature dependence magnetization follows crystallization kinetics revealed by DSC and XRD analysis. The TMA curve of the as-synthesized product exhibited a magnetic behavior of amorphous Ln–TM–B (amorphous Nd–Fe–B phase, $T_c = 140$ °C) along with the Fe–B (i.e. 490 °C « T_c « 600 °C) phase. The formation of the intermetallic $Nd_2Fe_{14}B$ phase ($T_c = 312$ °C) after reductive annealing is clear from the TMA curve presented in Fig. 9b.[3,17] However, during the high temperature reduction process, apart from the reduction of lanthanum oxide and its diffusion into the primary phase (Fe–B) to form a ternary $Nd_2Fe_{14}B$ compound, the stoichiometrically excess Fe in the α-Fe magnetic phase ($T_c = 760$ °C) remains in the final product. We are working on the optimization of the synthesis process to eliminate this excess Fe from the final product.

As can be seen from the XRD patterns (Fig. 4), the as-synthesized Nd–Fe–B nanoclusters are amorphous in nature. However, on reductive annealing at 950 °C apart from reducing the oxides, inter-diffusion of the elements takes place, resulting in the formation of oxygen free crystalline $Nd_2Fe_{14}B$, as has been observed by Sun et al.[5a] Appearance of sharp diffraction

peaks corresponding to the $Nd_2Fe_{14}B$ phase in the sample reductively annealed at 950 °C indicates that the temperature is suitable for reduction of oxides and interface diffusion of elements leading to the formation of a $Nd_2Fe_{14}B$ phase as has been shown schematically in Fig. 9.

Our synthesis process demonstrates a direct pathway for obtaining ternary inter-metallic nanoclusters with outstanding magnetic properties without using their micrometer sized oxide precursors and subsequent thermal treatments in the presence of CaH_2. The nanometer sized primary particles fabricated in our synthesis process certainly have a higher reduction rate than the conventional micrometer sized oxide precursors.

Conclusions

In summary, we have developed a facile, one-pot chemical synthesis process for Nd–Fe–B nanoclusters with oxygen bridging, which overcomes the reduction problem of lanthanide cations of highly negative reduction potential, the main hindrance for the fabrication of inter-metallic permanent magnets. The oxygen bridging between the Nd^{3+} ions and the negatively charged surface of the preformed Fe–B particles allows the conversion of Nd^{3+} cations into Nd. The resulting amorphous soft-magnetic nanoclusters can be transformed to the crystalline ferromagnetic $Nd_2Fe_{14}B$ phase with high coercivity and high saturation magnetization through reductive annealing at high temperature. While the oxygen-bridging between Ln cations and primary particles is of significant importance for binding the Ln ions on the primary particle surface, a high temperature reductive annealing process is essential for the inter-diffusion of the elements and reduction of their oxides to form pure inter-metallic nanostructures.

Acknowledgements

Notes and references

1 (a) O. Gutfleisch, M. A. Willard, E. Brück, C. H. Chen, S. G. Sankar and J. P. Liu, *Adv. Mater.*, 2011, **23**, 821; (b) Z. Shen, G. Zhang, H. Zhou, P. Sun, B. Li, D. Ding and T. Chen, *Adv. Mater.*, 2008, **20**, 984; (c) S. Heer, K. Kömpe, H.-U. Güdel and M. Haase, *Adv. Mater.*, 2004, **16**, 2102; (d) R. Yu, K. Yu, W. Wei, X. Xu, X. Qiu, S. Liu, W. Huang, G. Tang, H. Ford and B. Peng, *Adv. Mater.*, 2007, **19**, 838; (e) F. Zhao, M. Yuan, W. Zhang and S. Gao, *J. Am. Chem. Soc.*, 2006, **128**, 11758.

2 (a) P. Wachter, *Handbook on the Physics and Chemistry of Rare Earths*, North-Holland Publishing Company, Amsterdam, 2nd edn, 1979; (b) L. Wang, R. Yan, Z. Huo, L. Wang, J. Zeng, J. Bao, X. Wang, Q. Peng and Y. Li, *Angew. Chem., Int. Ed.*, 2005, **44**, 6054.

280 | *J. Mater. Chem. C*, 2013, **1**, 275–281

This journal is © The Royal Society of Chemistry 2013

3 (a) G. C. Hadjipanayis, *J. Magn. Magn. Mater.*, 1999, **200**, 373; (b) J. J. Croat, J. F. Herbst, R. W. Lee and F. E. Pinkerton, *J. Magn. Magn. Mater.*, 1999, **200**, 373; (c) Y. Hou, Z. Xu, S. Peng, C. Rong, J. P. Liu and S. Sun, *Adv. Mater.*, 2007, **19**, 3349; (d) Y. Hou, S. Sun, C. Rong and J. P. Liu, *Appl. Phys. Lett.*, 2007, **91**, 153117; (e) H. Zhang, S. Peng, C.-B. Rong, J. P. Liu, Y. Zhang, M. J. Kramer and S. Sun, *J. Mater. Chem.*, 2011, **21**, 16873.

4 (a) M.-P. Pileni, *Nanocrystals Forming Mesoscopic Structures*, Wiley-VCH, Weinheim, 2006; (b) G. Schmid, *Nanoparticles: From Theory to Application*, Wiley-VCH, Weinheim, 2004; (c) J. Park, K. An, Y. Hwang, J.-G. Park, H.-J. Noh, J.-Y. Kim, J.-H. Park, N.-M. Hwang and T. Hyeon, *Nat. Mater.*, 2004, **3**, 891; (d) W. S. Seo, H. H. Jo, K. Lee, B. Kim, S. J. Oh and J. T. Park, *Angew. Chem., Int. Ed.*, 2004, **43**, 1115; (e) M. Monge, M. L. Kahn, A. Maisonnat and B. Chaudret, *Angew. Chem., Int. Ed.*, 2003, **42**, 5321; (f) L. Gou and C. J. Murphy, *Nano Lett.*, 2003, **3**, 231.

5 (a) S. Sun, C. B. Murray, D. Weller, L. Folks and A. Moser, *Science*, 2000, **287**, 1989; (b) H. Zeng, J. Li, Z. L. Wang, J. P. Liu and S. Sun, *Nature*, 2002, **420**, 395; (c) C. Wang, Y. Hou, J. Kim and S. Sun, *Angew. Chem., Int. Ed.*, 2007, **46**, 6333.

6 (a) E. V. Shevchenko, D. V. Talapin, N. A. Cotov, C. B. Murray and S. O'Brien, *Nature*, 2006, **439**, 55; (b) E. V. Shevchenko, D. V. Talapin, C. B. Murray and S. O'Brien, *J. Am. Chem. Soc.*, 2006, **128**, 3620.

7 (a) X. Wang, X.-M. Sun, D. Yu, B.-S. Zou and Y. Li, *Adv. Mater.*, 2003, **15**, 1442; (b) M. Yada, M. Mihara, S. Mouri, M. Kuroki and T. Kijima, *Adv. Mater.*, 2002, **14**, 309.

8 (a) B. L. Cushing, V. L. Kolesnichenko and C. O'Connor, *Chem. Rev.*, 2004, **104**, 3893; (b) C. G. Hadjipanayis, M. J. Bonder, S. Balakrishnan, X. Wang, H. Mao and G. C. Hadjipanayis, *Small*, 2008, **4**, 1925.

9 (a) C. W. Kim, U. Pal, S. Park, J. Kim and Y. S. Kang, *Chem.–Eur. J.*, 2012, **18**, 12314; (b) Y. H. Kim, D. K. Lee, H. G. Cha, C. W. Kim and Y. S. Kang, *J. Phys. Chem. B*, 2007, **111**, 3629; (c) Y. H. Kim, D. K. Lee, H. G. Cha, C. W. Kim, Y. C. Kang and Y. S. Kang, *J. Phys. Chem. B*, 2006, **110**, 24923.

10 (a) X. Wang and Y. Li, *Angew. Chem., Int. Ed.*, 2002, **41**, 4790; (b) F. Bouyer, N. Sanson, M. Destarac and C. Gerardin, *New J. Chem.*, 2006, **30**, 399; (c) B. Hou, Y. Xu, D. Wu and Y. Sun, *J. Mater. Sci.*, 2007, **42**, 1397.

11 (a) A.-H. Lu, E. L. Salabas and F. Schűth, *Angew. Chem., Int. Ed.*, 2007, **46**, 1222; (b) J. Park, J. Joo, S. G. Kwon, Y. Jang and T. Hyeon, *Angew. Chem., Int. Ed.*, 2007, **46**, 4630.

12 (a) J. F. Moulder, W. F. Stickle, P. E. Sobol and K. D. Bomben, *Handbook of X-Ray Photoelectron Spectroscopy: A Reference Book of Standard Spectra for Identification and Interpretation of XPS Data, Physical Electronics*, 1995; (b) B. V. Crist, *Handbook of Monocromatic XPS Spectra: The Elements and Native Oxides*, John Willey and Sons Ltd, Chichester, 2000.

13 (a) T. L. Barr, *J. Phys. Chem.*, 1978, **82**, 1801; (b) M. Mullet, V. Khare and C. Ruby, *Surf. Interface Anal.*, 2008, **40**, 323.

14 (a) V. Dimitrov and T. Komatsu, *J. Solid State Chem.*, 2002, **163**, 100; (b) T. L. Barr, *Modern ESCA; The Principles and Practice of X-Ray Photoelectron Spectroscopy*, CRS Press, Boca Raton, FL, 1994.

15 P. K. Deheri, V. Swaminathan, S. D. Bhame, Z. Liu and R. V. Ramanujan, *Chem. Mater.*, 2010, **22**, 6509.

16 W. Gong, G. C. Hadgipanayis and R. F. Krause, *J. Appl. Phys.*, 1994, **75**, 6649.

17 (a) N. Oono, H. Nitta and Y. Iijima, *Mater. Trans.*, 2003, **44**, 2078; (b) T. V. Rajan, C. P. Sharma, A. Sharma, *Heat Treatment: Principals and Techniques*, PHI Learning Pvt. Ltd, New Delhi, 2nd edn, 2011.

This journal is © The Royal Society of Chemistry 2013

J. Mater. Chem. C, 2013, **1**, 275–281 | **281**